ceramics

MDPI

Article

Barium Silicate Glasses and Glass–Ceramic Seals for YSZ-Based Electrochemical Devices

Alyona Vepreva [1], Dmitry Dubovtsev [1], Daria Krainova [1], Yulia Chetvertnykh [1], Semyon Belyakov [2], Nailya Saetova [1,3] and Anton Kuzmin [1,3,*]

[1] Institute of Chemistry and Ecology, Vyatka State University, Kirov 610000, Russia; a.vepreva98@mail.ru (A.V.); d.dubovtzev@yandex.ru (D.D.); dashakraynova@yandex.ru (D.K.); usr22050@vyatsu.ru (Y.C.); n.saetova@yandex.ru (N.S.)

[2] Laboratory of Kinetics, Institute of High-Temperature Electrochemistry, Ural Branch of Russian Academy of Sciences, Yekaterinburg 620137, Russia; bca2@mail.ru

[3] Laboratory of Solid State Chemistry, Institute of Solid State Chemistry and Mechanochemistry, Siberian Branch of Russian Academy of Sciences, Novosibirsk 630128, Russia

* Correspondence: a.v.kuzmin@yandex.ru

Abstract: The effect of partial SiO_2 substitution with Al_2O_3 and B_2O_3 on the thermal properties and crystallization of glass sealants in the $(50 - x)SiO_2$–30BaO–20MgO–$xAl_2O_3(B_2O_3)$ (wt %) system is studied. It is established that the coefficient of thermal expansion of all obtained glasses lies within a range of 8.2–9.9 $\times 10^{-6}$ K^{-1}. Alumina-doped glasses crystallize after quenching, while samples containing boron oxide are completely amorphous. Magnesium silicates are formed in all glasses after exposure at 1000 °C for 125 h. After 500 h of exposure, a noticeable diffusion of zirconium ions is observed from the YSZ electrolyte to the glass sealant volume, resulting in the formation of the $BaZrSi_3O_9$ compound. The crystallization and products of interaction between YSZ ceramics and boron-containing sealants have no significant effects on the adhesion and properties of glass sealants, which makes them promising for applications in electrochemical devices.

Keywords: glass; glass–ceramic; sealant; yttria-stabilized zirconia; microstructure; crystallization; SOFC

Citation: Vepreva, A.; Dubovtsev, D.; Krainova, D.; Chetvertnykh, Y.; Belyakov, S.; Saetova, N.; Kuzmin, A. Barium Silicate Glasses and Glass–Ceramic Seals for YSZ-Based Electrochemical Devices. *Ceramics* **2023**, *6*, 1314–1329. https://doi.org/10.3390/ceramics6030081

Academic Editors: Georgiy Shakhgildyan and Michael I. Ojovan

Received: 22 May 2023
Revised: 17 June 2023
Accepted: 20 June 2023
Published: 22 June 2023

1. Introduction

Yttria-stabilized zirconia (YSZ) is widely used for various high-temperature devices, including gas sensors [1,2], fuel cells [3], and electrolyzers [4]. YSZ-based gas sensors are applied in various fields from medicine to the control of vehicle exhaust emissions [5] due to the high sensitivity to such gases as NO_x, CO, H_2, and hydrocarbons [6]. High-temperature annealing is frequently used to combine the sensor's parts [7] and create tight contact. Another approach to sensor assembling implies the application of inorganic binders, mainly a mixture of liquid glass and alumina powder [5,8]. Despite the fact that glass sealants are the least spread for electrochemical sensors, there are some studies indicating the perspective of such an approach [9]. In addition, glass sealants are the most suitable for sensors operating at high (above 1000 °C) temperatures, which is confirmed by the latest developments of the company Schott (Germany) (one of the largest sealant manufacturers on the international market), who presented a high-temperature sensor for monitoring the composition of car exhaust gases, assembled using a glass–ceramic sealant (data on the glass–ceramic high-temperature sealant HEATEN produced by Schott (Germany) can be found at https://www.schott.com/en-gb/products/heatan-p1000279/technical-details?tab= e5001c8e5b8b497997de6e65e33174f5, accessed on 21 June 2023).

As mentioned above, YSZ is widely used for a number of high-temperature devices, including oxygen pumps [10,11]. Oxygen pumps require tight sealing that can be reached by glass application [12–14]. In addition, high-temperature glass and glass–ceramic sealants

are required to seal laboratory cells when conducting different experiments [15,16]. In addition to oxygen pumps, solid oxide fuel cells (SOFCs) are one of the common high-temperature devices widely using glasses and glass–ceramics as sealing materials [3].

Barium silicate glasses are the most widespread glass and glass–ceramic sealants due to their good stability at high temperatures, high mechanical strength, appropriate coefficient of thermal expansion, and low electrical conductivity [17–19]. The properties of glass sealants can be controlled by changing the glass composition [20–22] and the introduction of filles into the glass matrix to obtain composites [19,23,24]. Several scientific groups studying barium-containing and barium-free glass sealants and led by the following scientists can be mentioned: K. Singh and G. Kaur [20,25,26], F. Smeacetto and A.G. Sabato [27–29], X. Wang and Y. Dong [19,30,31], and A. Kuzmin and N. Saetova [32–35]. However, the sealant compositions presented in the cited studies are complex and contain more than four oxides. In this study, we aimed to develop glass sealants of less complex compositions containing three main oxides (SiO_2, BaO, and MgO) and small amounts of additives (to 4 wt %). In addition, the developed glass sealants are expected to be used not only for SOFC joints, but for sealing oxygen pumps, which can be sealed at higher temperatures than SOFCs.

The choice of glass components is conditioned by their role in the glass network and their effect on glass properties. Thus, SiO_2 is a glass former [22,36], and BaO and MgO are modifiers increasing glass transition and softening temperatures, which is vital for high-temperature applications and CTE value [22,36]. B_2O_3 (a glass-forming oxide) was added to improve wettability and suppress crystallization [20,36]. Al_2O_3, which can act as both a glass former and modifier depending on the concentration, was also introduced to suppress crystallization [20,36] and increase the long-term stability of the sealant [22,36]. The introduction of small amounts of additives is believed not to affect the glass properties dramatically (for instance, CTE and sealing temperature), but to impact the crystallization behavior of glasses and their stability under high temperatures. It should also be mentioned that, unlike other studies [37–40], the sealants under investigation contain both BaO and MgO.

This work is devoted to the investigation of the effect of the partial substitution of silica in the $(50 - x)SiO_2$–30BaO–20MgO–$xAl_2O_3(B_2O_3)$ (wt %) with Al_2O_3 and B_2O_3 on the thermal properties and crystallization of glass–ceramic sealants for high-temperature applications. The choice of glass composition is based on previous studies that utilized the $45SiO_2$–$15Al_2O_3$–25BaO–15MgO (wt %) glass for oxygen pump sealing [41].

2. Materials and Methods

$(50 - x)SiO_2$-30BaO-20MgO-xAl_2O_3/B_2O_3 (wt %) glasses were obtained by melting the stoichiometric mixtures of SiO_2, $BaCO_3$, $MgCO_3$, Al_2O_3, and B_2O_3 (99.99% purity) in alundum crucibles at a temperature of 1500 °C, followed by pouring the melt into a glassy- carbon mold. Annealing was performed at a temperature of T_g—50 °C for 1 h, and then the glass was cooled naturally in a furnace to room temperature. The chemical composition of the obtained glasses was determined by atomic emission spectroscopy (AES) using an Optima 4300 DV (Perkin Elmer, Waltham, MA, USA) spectrometer with an accuracy of 2–3%. The phase composition of the glasses and glass–ceramics was studied by X-ray diffraction (XRD) using an XRD-7000 (Shimadzu, Kyoto, Japan) and a D/MAX-2200 (Rigaku, Tokyo, Japan) diffractometer with Cu-K_α (λ= 1.5418 Å) radiation. XRD patterns were collected at room temperature in a 2θ range from 10 to 80° with a scanning step of 2 °/min.

To study the thermal expansion of the obtained materials, samples were cut out of as-cast glasses and glass–ceramic samples were prepared by the compaction of glass powders followed by sintering at 1050 °C. The measurements were conducted in temperature ranges of 50–800 °C (cut samples) and 50–720 °C (compacted samples) using a quartz dilatometer with a TT-80 (Tesatronic, Renens, Switzerland) meter with an accuracy of 0.01 μm; the heating rate was 2 °/min.

Hot-stage microscopy (HSM) was applied to study the sealant behavior under heating by means of an ODP 868 (TA Instruments, New Castle, DE, USA) optical dilatometry platform; the measurements were conducted in a heating microscope mode with a rate of 2 °/min. Samples were obtained by the compaction of glass powders; YSZ ceramic was used as a substrate. The glass transition and crystallization temperatures were determined by differential scanning calorimetry (DSC) using a 449 F1 Jupiter (Netzsch, Selb, Germany) simultaneous thermal analysis device. The following measurement conditions were set: platinum crucibles, a temperature range of 35–1100 °C, air atmosphere, and a heating rate of 10 °/min.

The glass powder mixed with ethyl alcohol was applied onto the YSZ surface to study the behavior of the sealant in contact with joined materials. Then, the samples were heat treated by the sealing mode (temperature of 1240 °C, 10 min, heating rate of 2 °/min) in an oxidizing atmosphere and cooled to room temperature in a furnace. The morphology of YSZ–sealant–YSZ sealed samples was studied by scanning electron microscopy (SEM) and energy dispersive spectroscopy (EDS) using a JSM-6510 LV (JEOL, Tokyo, Japan) microscope equipped with an Inca Energy 350 (Oxford Instruments, Abingdon, UK) energy dispersive spectroscopy system with an X-max 80 detector. Cross sections of samples were obtained by epoxy impregnation, followed by grinding and polishing using a P12Sb (Polilab, Moscow, Russia). SEM images were obtained in backscattered electron (BSE) mode to provide a contrast between the glass matrix and crystallized phases.

3. Results and Discussion

Table 1 presents the nominal glass compositions and those determined by AES. In general, the real compositions of the glasses are close to the nominal ones and the differences are within the method error. However, there is an interaction between alundum crucibles and glass melts, which is seen in the Al_2O_3 content.

Table 1. Nominal and real (AES) compositions of glasses in the $(50 - x)SiO_2$-30BaO-20MgO-$xAl_2O_3(B_2O_3)$ system (wt %).

Sample	SiO_2	MgO	BaO	Al_2O_3	B_2O_3
3B	47.0	20.0	30.0	-	3.0
3B AES	**46.3**	**17.9**	**31.4**	**1.8**	**2.6**
3A	47.0	20.0	30.0	3.0	-
3A AES	**43.9**	**20.2**	**32.1**	**3.8**	**-**
4B	46.0	20.0	30.0	-	4.0
4B AES	**45.7**	**21.7**	**27.4**	**1.6**	**3.6**
4A	46.0	20.0	30.0	4.0	-
4A AES	**44.9**	**18.4**	**31.8**	**4.9**	**-**

The XRD patterns given in Figure 1 demonstrate a broad halo typical of glasses. The appearance of a less pronounced halo near 40° in addition to the main halo observed in an angle range of ~20–30° could be connected with a phase separation [42].

After quenching, the samples doped with alumina demonstrated visible separation in the transparent (lower part) and opaque (upper part) layers, which is schematically demonstrated in Figure 1. To determine the phase composition of each part, the obtained glasses were cut, the separated parts were powdered, and XRD patterns were then collected (these patterns are given in Figure 1). According to the XRD patterns collected from the transparent and opaque regions of 4A glass (Figure 1), some XRD peaks indicating the presence of crystalline phases are seen in the opaque glass, while its transparent part is amorphous. The crystalline phase can be identified as magnesium silicate Mg_2SiO_4 (PDF card no. #078-1369). Glasses doped with boron oxide were homogeneous and transparent and demonstrated no visible phase separation or crystallization.

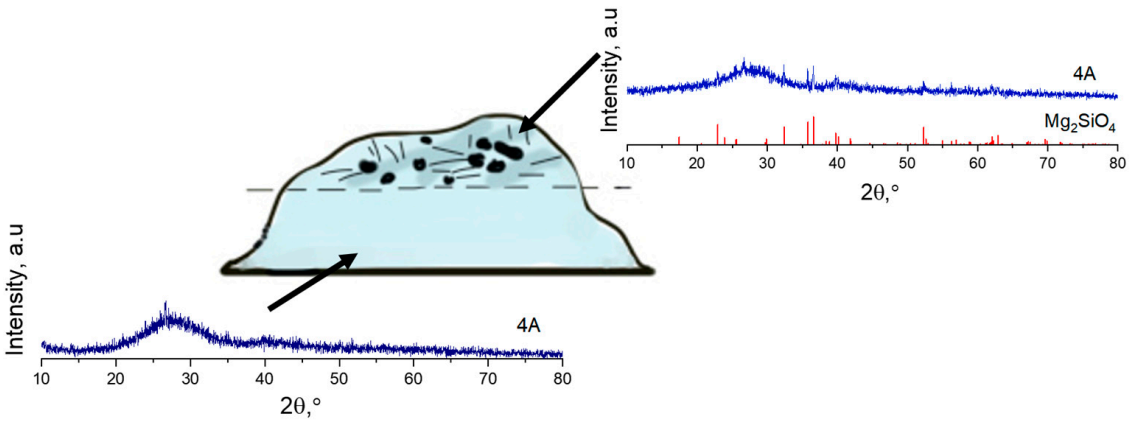

Figure 1. XRD patterns of as-cast $46SiO_2$-30BaO-20MgO-$4Al_2O_3$ glass taken in different glass areas.

To obtain detailed information regarding phase separation in the 4A sample, its cross-section was studied by means of SEM and EDX. Figure 2a,b present SEM images with clearly pronounced areas in the glass volume consisting of needle-like crystals and broad light and dark bands. Since the images were obtained in the backscattered electron (BSE) mode, it can be assumed that the chemical composition of the mentioned regions differs, which is confirmed by the EDX mapping data. Since this method is insensitive to boron, some inaccuracies might appear during the EDX study. However, considering that the maximum boron content in the studied glasses is 4 wt % and EDX is the only method that can be used to characterize the phase composition of sealed glasses near the sealant–material interface, it was assumed that, in this case, boron could be excluded from further consideration without any significant loss in accuracy.

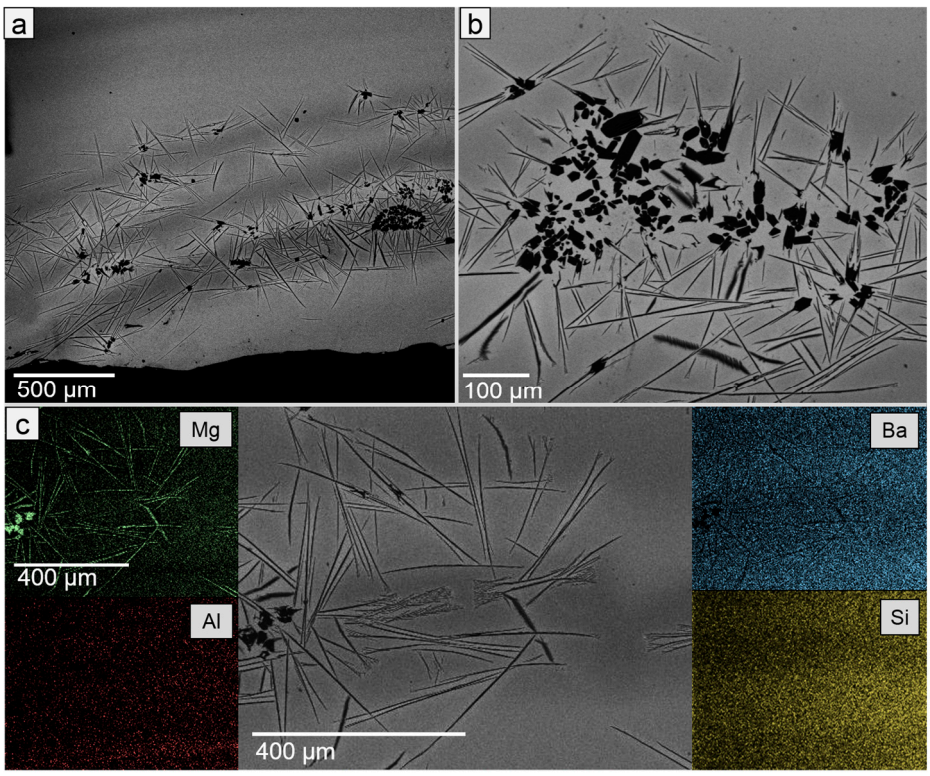

Figure 2. SEM images and element distribution maps for 4A as-cast glass: a – scale 500 µm, b – scale 100 µm, c – SEM images and element distribution maps. The scale of all maps is the same.

As seen in the element distribution maps given in Figure 2c, needle-like crystals can be attributed to manganese compounds, which correlated with XRD data (Figure 1), darker areas are enriched with silicon, and lighter areas possess an increased barium content. Thus, it is obvious that phase separation and crystallization occur during melt cooling after quenching. The boron-containing glasses do not show phase separation and crystallization after melt cooling.

When glasses are used as sealing materials, the thermal properties of the materials being joined and the operation temperatures must be considered. In this study, the sealants have been developed to join construction elements made of YSZ ceramics for which the value of the coefficient of thermal expansion (CTE) is ~9–10 $\times$ 10^{-6} K^{-1} [32]; this ceramic is used for oxygen pumps and sensors operating at rather high temperatures up to 1100 °C. The thermal characteristics of the glasses determined by DSC, dilatometry, and hot-stage microscopy are given in Table 2. It should be mentioned that the softening temperature (T_s) determined by HSM is surprisingly high and its value is far beyond the range between T_g and T_c, which is typical of glasses [43]. This might be explained by the crystallization of the studied samples during slow heating (2 °/min), leading to shifting all characteristic temperatures towards high temperatures.

Table 2. Thermal properties of $(50 - x)SiO_2$-30BaO-20MgO-$xAl_2O_3(B_2O_3)$ (wt %) glasses.

Sample	HSM, °C (±10 °C)	DSC, °C (±2 °C)		CTE $\times$ 10^{-6} K^{-1} (±0.1)	
	T_S	T_g	T_c	Bulk	Pressed
3A	1170	740	915	8.4	9.4
4A	1130	740	930	8.7	8.2
3B	1150	725	910	8.3	9.5
4B	1200	720	925	9.5	9.9

T_S—softening temperature.

As seen in the DSC data, the glass transition temperatures (T_g) of the boron-containing glasses are lower than those of the glasses doped with alumina. An increase in the content of both boron and aluminum oxides results in a slight growth of the crystallization temperature (T_c). It should be mentioned that in all cases, the crystallization temperatures are significantly lower than presumable operating temperatures; therefore, intense crystallization might be expected during sealing and running.

Figure 3 presents the temperature dependences of the linear expansion of YSZ ceramics, as-cast glasses, and glass–ceramic samples obtained by pressing glass powders followed by sintering at 1050 °C. Typical dilatometric curves of as-cast glasses are shown in the example of 4A and 4B samples. Given that glasses usually soften at lower temperatures than glass–ceramics, the measurements of the glass samples were carried out in a narrower temperature range. In general, all studied glass sealants have good compatibility with YSZ ceramics in terms of thermal expansion. It should be mentioned that in the studied temperature range, a dome typical for the dilatometric curves of glasses is seen only for the 4B glass, which might be connected with the insufficient maximum temperature of the experiment or with the partial crystallization of the glasses during heating, which affects the curve shape. The values of CTE given in Table 2 were calculated in a temperature range of 50–500 °C. The CTE values of the glass–ceramic samples are slightly higher than those of glasses in most cases, except for the 4A composition. A greater CTE value of glass (8.7 $\times$ 10^{-6} K^{-1}) compared with glass–ceramics (8.2 $\times$ 10^{-6} K^{-1}) might be connected with the appearance of crystalline phases with a low CTE value during the glass–ceramics sample preparation.

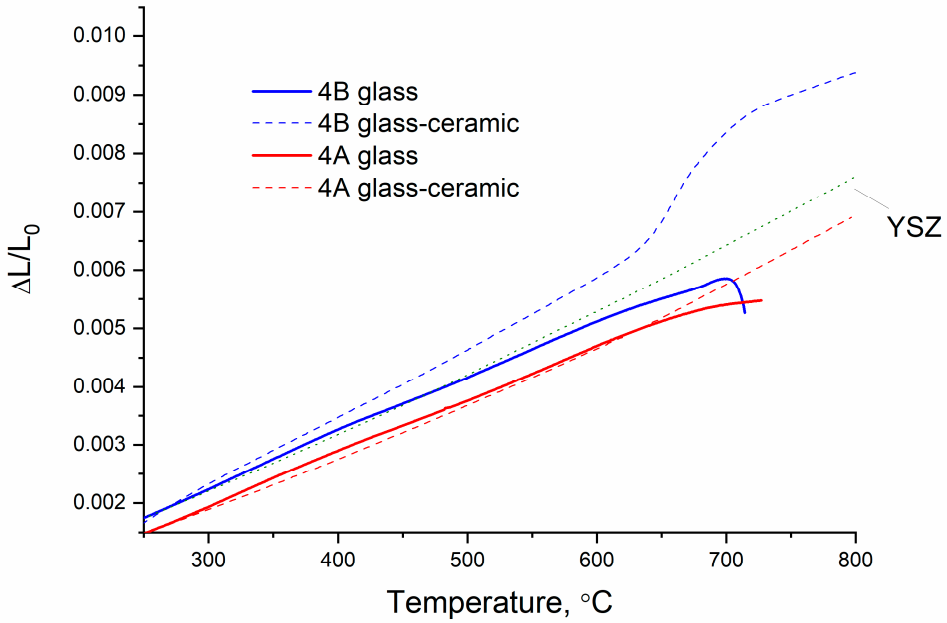

Figure 3. Curves of relative elongation of as-cast glasses, glass–ceramics, and YSZ ceramics.

According to XRD patterns collected after the sintering of pressed samples at 1050 °C (Figure 4), the 3B sample demonstrates the lowest tendency to crystallization: its crystallization degree was 15.1%, while that value was 79.2, 62.3, and 69.7 for samples 3A, 4A, and 4B, respectively. The percentage of crystalline phases was roughly estimated using the method described by Pardo [44] with an accuracy of ±2.5%. According to the phase identification, $BaMg_2Si_2O_7$ (CTE~10 × 10^{-6} K^{-1}) [45], $MgSiO_3$, and Mg_2SiO_4 were found.

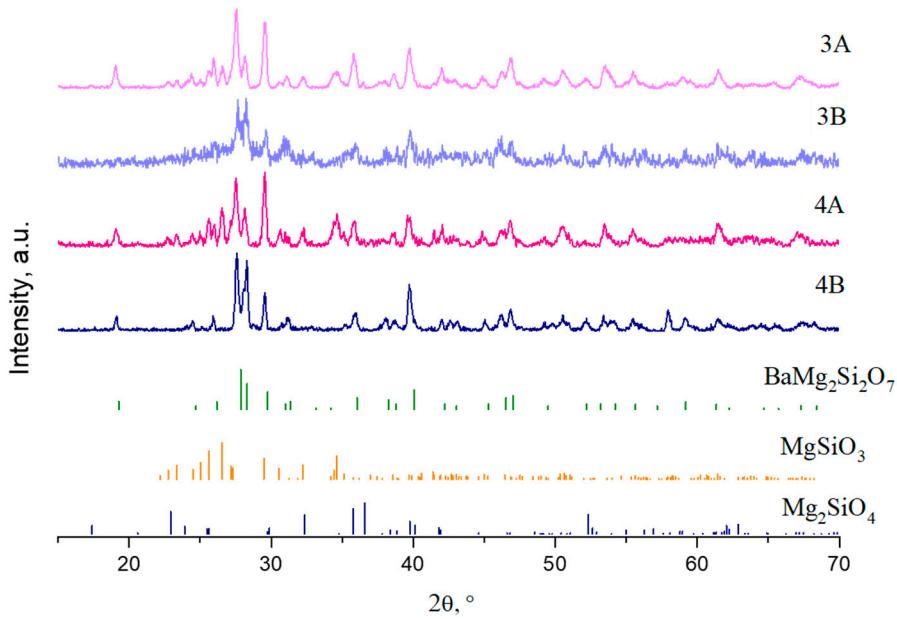

Figure 4. XRD patterns of $(50 - x)SiO_2$-30BaO-20MgO-$xAl_2O_3(B_2O_3)$ glasses sintered at 1050 °C for 10 min. $BaMg_2Si_2O_7$ (PDF#10-0044), $MgSiO_3$ (PDF#018-0778), Mg_2SiO_4 (PDF#078-1369).

The behavior of the glasses under heating was studied using hot-stage microscopy, allowing the tracking of sintering, softening, sphere formation, and melting [46]. However, only the sintering temperature can be clearly determined for the studied samples, while further shape change is less pronounced. As seen in the HSM images given in Figure 5,

the formation of a sphere typical of glasses [43,47,48] was not observed for some samples, and a shape change corresponding to melting appears after softening. This might be connected with the fact that the softening temperature (1140–1200 °C) is higher than the crystallization temperature (Table 2) and glass–ceramic samples with a high crystallinity degree are formed, which affects the sample behavior under heating.

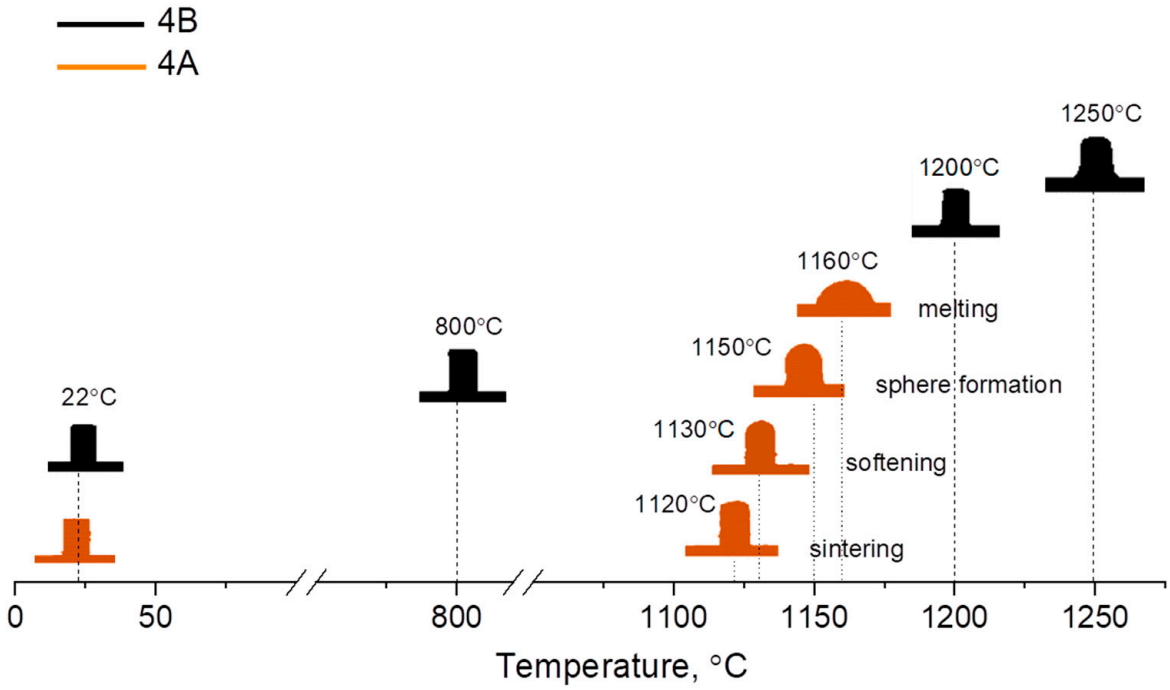

Figure 5. Hot-stage microscopy images for 4B and 4A samples.

As a rule, the sealing temperature is chosen based on the hot-stage microscopy data (when this method is used), and two approaches to its choice can be considered. If the sphere formation temperature is chosen as the sealing temperature, the sealing time is increased; if the half-sphere formation temperature is chosen as the sealing one, the sealing time is reduced [49]. However, this is impossible for the glasses under investigation due to intense crystallization causing the unusual behavior described above. Therefore, a temperature of 1240 °C was chosen empirically (based on the results of the experiment consisting of the measurement of wettability angles using cross-sections of YSZ–sealant samples [50]); the same sealing temperature was used for all glasses to reliably compare their crystallization during heat treatment.

Figure 6 presents the typical XRD patterns of YSZ–sealant on the examples of samples containing 3 wt % Al_2O_3 and B_2O_3. The samples were treated by the sealing mode: heating to 1240 °C with a rate of 2 °/min, exposing for 10 min, and natural cooling to room temperature. Then, the samples were put in a furnace, heated to 1000 °C, and kept for 125, 500, and 1000 h. As is seen, the main crystallization occurred during 125 h of exposure, which is typical for glasses [28,51,52], and further exposure did not lead to noticeable changes in the XRD patterns. The XRD peaks were attributed to enstatite ($MgSiO_3$), forsterite (Mg_2SiO_4), and YSZ substrate (30, 50, and 60°). It is worth noting that the $BaMg_2Si_2O_7$ compound found after sample sintering for CTE measurements (Figure 4) was not observed, which might be connected with its instability under sealing conditions. It should be noted that barium silicate glasses tend to the formation of numerous phases during crystallization, which could undergo phase transitions [51,53,54]. Therefore, the phase identification in such glasses using only XRD analysis is complicated.

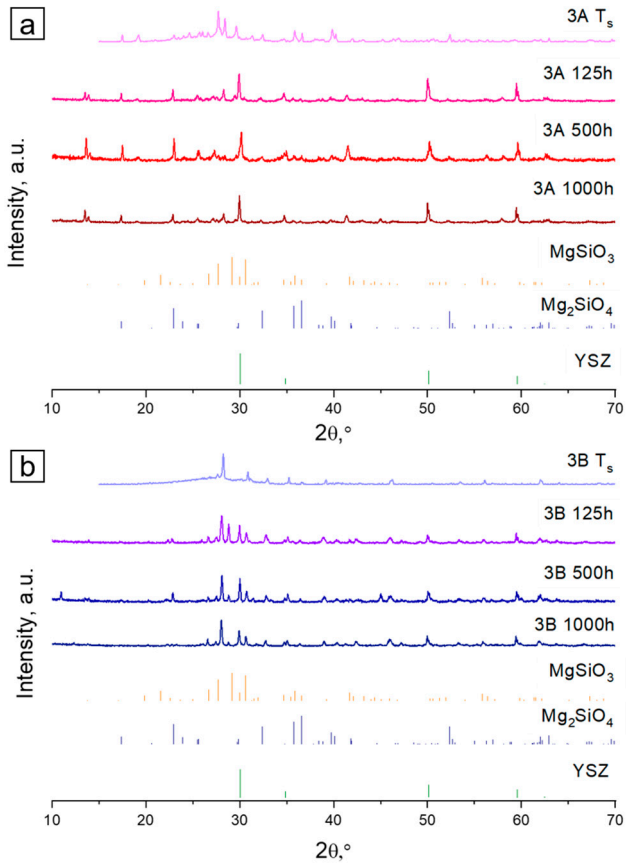

Figure 6. XRD patterns of YSZ–sealant samples of 3A (**a**) and 3B (**b**) glasses after heat treatment by the sealing mode and exposure for 125, 500, and 1000 h at 1000 °C in air atmosphere. $MgSiO_3$ (PDF#018-0778), Mg_2SiO_4 (PDF#078-1369).

To study the chemical interaction and crystallization processes, cross-sections of YSZ–sealant samples were prepared. The microstructure was studied by scanning electron microscopy in BSE mode because it is sensitive to the atomic weight of elements, and the crystalline phases of different compositions can be distinguished by contrast.

Figure 7 shows the SEM images and element distribution maps of YSZ–4A and YSZ–4B samples exposed at 1000 °C for 125 h. The observed inhomogeneity of the element distribution is caused by the crystallization and phase separation typical for barium-containing glasses [55] and demonstrated above for alumina-doped samples (Figure 2). In the presented SEM images, phase separation in glasses is seen from a slight difference in gray shadows: darker irregular areas can be distinguished in the light-gray glass (examples of such areas are highlighted in Figure 7). Thus, the darker area near point 1 (Figure 7a) is enriched with alumina (Table S1) while, the lighter area near point 3 is enriched with barium. It was also found that in boron-containing samples 3B and 4B, $MgSiO_3$ is formed (Figure 7a, point 2), while both Mg_2SiO_4 and $MgSiO_3$ appear in alumina-containing glasses (Figure 7a, spectrum 2 (Table S1) and Figure 8, spectra 6 and 7, Table S1).

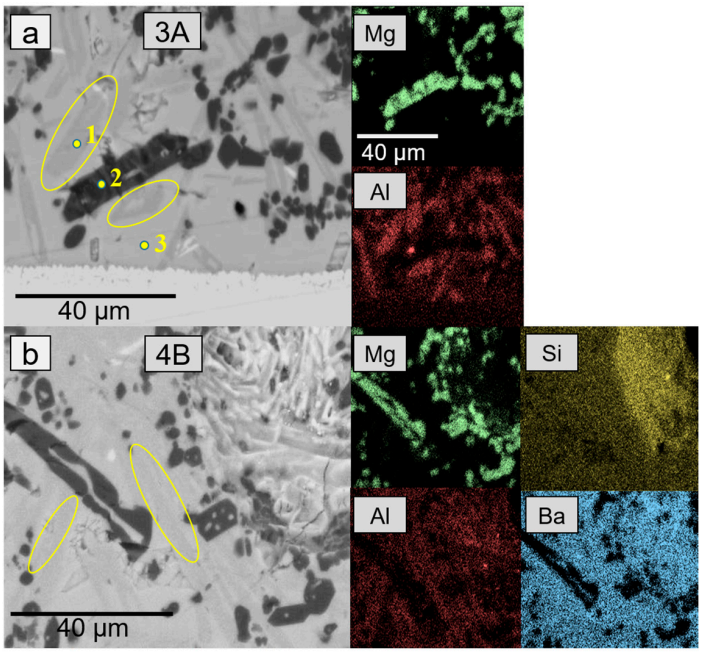

Figure 7. SEM images and element distribution maps of YSZ–3A (**a**) and YSZ–4B (**b**) joints after exposure at 1000 °C for 125 h in air atmosphere. Points 1–3 indicate areas of EDX study (chemical compositions are given in Table S1). Yellow circles indicate areas with increased alumina content. The scale of all element distribution maps is similar.

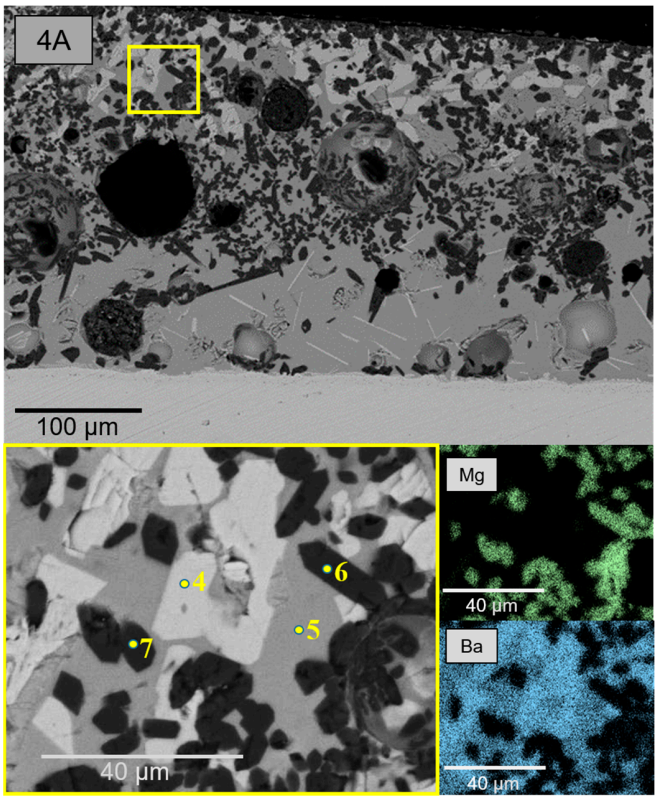

Figure 8. SEM images and element distribution maps of YSZ–4A joint after exposure at 1000 °C for 125 h in air atmosphere. Points 4–7 indicate areas of EDX study (chemical compositions are given in Table S1). Yellow square indicates the area of the upper SEM image given in higher magnification.

After exposure of the YSZ–4A sample for 125 h (Figure 8), areas with different chemical compositions are observed in BSE SEM images. For this composition, uneven phase distribution is typical: the composition of lighter areas (Figure 8, spectrum 1) is close to the $BaSi_2O_5$ compound (which can be both amorphous [56] and crystalline) and these areas are located near the sealant surface. The composition of the dark crystals of similar shape (spectra 6 and 7, Table S1) is close to the $MgSiO_3$ phase. It should be noted that no alumina-containing phases were found, which might indicate that it does not contribute to the phase formation. However, it should be mentioned that since the alumina content in the studied glass is low (4 wt %), aluminum-containing crystalline phases could be distributed unevenly and its presence might be missed due to the SEM limitations connected with the visible area. A thin uniform layer and needle-like crystals are observed near the sealant–YSZ interface, but their composition cannot be determined by EDX due to the small size.

Figure 9 shows SEM images of YSZ–sealant cross-sections after 500 h exposure at 1000 °C. Triangle-shaped light inclusions are observed in 3B and 4B sealants (Figure 9a, point 1) in addition to magnesium silicate crystals observed after 125 h exposure. Using EDX data, it was established that the chemical composition in point 1 (Figure 9) is close to the $BaZrSi_3O_9$ compound (experimental and theoretical compositions are given in Table 3). In addition, some amounts of yttria and zirconia were found in the glass volume (point 2). Obviously, both elements were transferred into the glass matrix due to ion diffusion from the YSZ ceramics during heat treatment. Although zirconium and yttrium diffusion was also observed in the case of the 3A and 4A sealants (Figure 9d, points 6 and 7), the formation of $BaZrSi_3O_9$ was not established. Some changes in magnesium silicate formation can be mentioned: while $MgSiO_3$ was formed in the 3B and 4B sealants boron-containing glasses after 125 h exposure, it was not found in the 3B sealant after 500 h exposure. Dark crystals seen in sealants 3A, 4A, and 3B (Figure 9, points 3 and 4) correspond to the Mg_2SiO_4 phase, while Mg_2SiO_3 is found in the 4B sample. According to the EDX analysis of residual glass (points 2, 5, 6, and 7), the glass matrix is depleted with magnesium and silicon, which is apparently caused by the intense crystallization of manganese silicates.

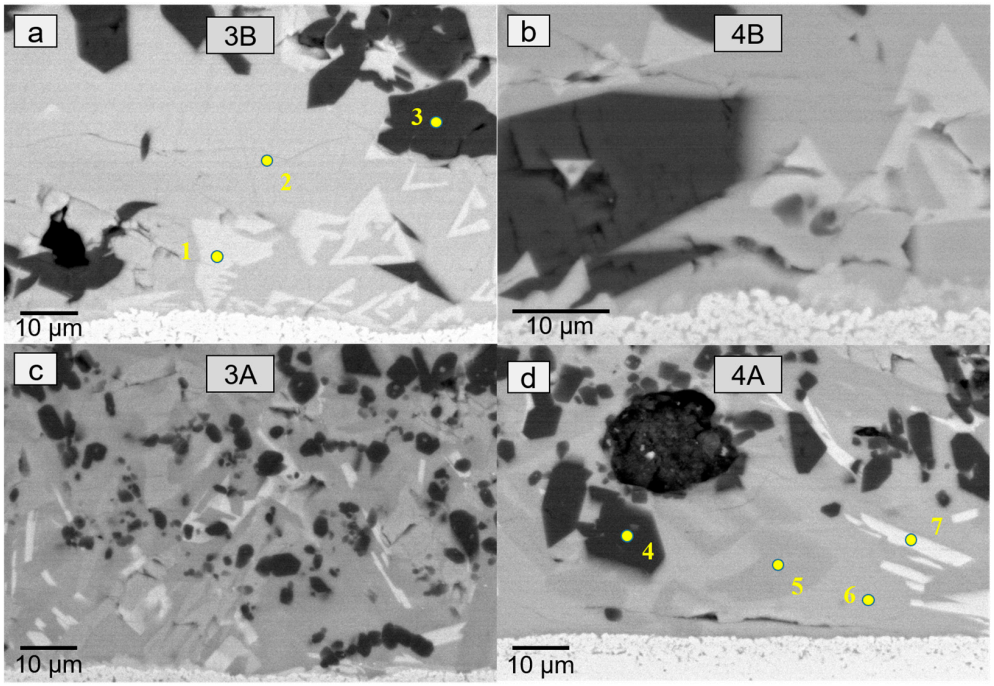

Figure 9. SEM images of sealant–YSZ interface after 500 h of exposure at 1000 °C in air atmosphere. Points correspond to the areas of EDX study: **a** – 3B sealant, **b** – 4B sealant, **c** – 3A sealant, and **d** – 4A sealant. Points 1–7 indicate areas of EDX study (chemical compositions are given in Table 3).

Table 3. Chemical composition determined by EDX in points depicted in Figure 9 (wt %) *.

Element (wt %)	Ba	Mg	Si	O	Al	Zr	Y
1	34.4	0.3	22.7	42.2	0.3	20.4	0.4
2	32.2	3.1	24.6	37.2	1.1	1.3	3.5
3	0.1	32.6	19.2	48.1	-	-	-
4	0.8	33.8	20.7	44.7	-	-	-
5	38.2	3.1	19.9	33.5	5.4	-	-
6	37.5	3.1	24.1	34.2	1.2	4.1	3.2
7	41.6	2.6	22.0	32.9	0.9	8.2	2.3
Mg_2SiO_4 **	**-**	**34.6**	**20.0**	**45.5**	**-**	**-**	**-**
$BaZrSi_3O_9$ **	**30.1**	**-**	**18.4**	**31.5**	**-**	**20.0**	**-**

*—excluding boron; **—theoretical values.

The further study of yttrium and zirconium diffusion to the glass volume was carried out using YSZ–sealant–YSZ joints kept at 1000 °C for 1000 h in an air atmosphere (Figure 10). According to the collected data, no new compounds were formed and the main crystalline phases are Mg_2SiO_4 and $BaZrSi_3O_9$ (Table S2). It is clearly seen that despite the similar phase composition, the distribution of the formed crystal over the glass volume differs for compositions substituted with boron and aluminum oxides. Thus, the magnesium silicate crystals formed in boron-containing glasses (Figure 10b) are larger compared with those in aluminum-containing glasses (Figure 10d), and are more evenly distributed over the glass volume. It should be noted that no $MgSiO_3$ crystals were observed after 1000 h exposure, which might be connected with the fact that, in terms of thermodynamics, Mg_2SiO_4 formation is preferable to $MgSiO_3$ formation [57–59]. As for the $BaZrSi_3O_9$ phase, it was only found in boron-containing glasses (Figure 10a,b). Although the size of the needle-like crystals located near alumina-doped sealant–YSZ interface increased, it is still insufficient to determine their chemical compositions using EDX.

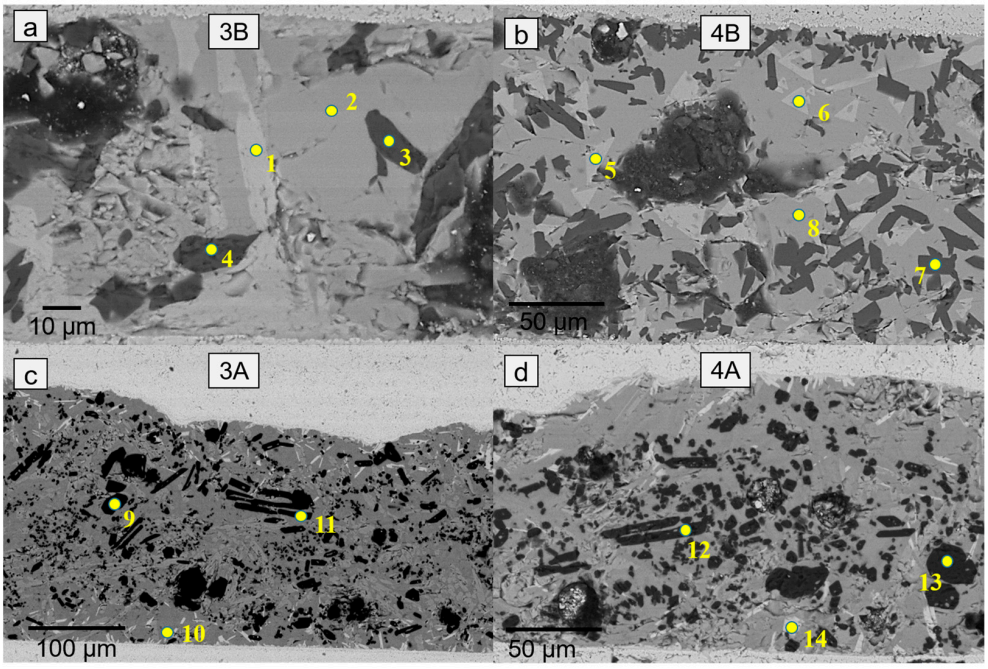

Figure 10. SEM images of YSZ–glass–YSZ joints after 1000 h exposure at 1000 °C in an air atmosphere: **a** – 3B sealant, **b** – 4B sealant, **c** – 3A sealant, and **d** – 4A sealant. Points correspond to the areas of EDX study; corresponding chemical compositions are given in Table S2.

To study the Zr^{2+} and Y^{3+} diffusion into the sealant volume, element distribution profiles were collected on the YSZ–3B (Figure 11a,c,d) samples after 125, 500, and 1000 h

exposure at 1000 °C and the YSZ–3A (Figure 11b) sample after 1000 h exposure at 1000 °C in an air atmosphere. As is seen, despite the diffusion, zirconium is unevenly distributed over the glass volume, which can be explained by its binding into silicates during its interaction with the glass network. Obviously, the formation of the Zr-containing phase becomes more pronounced with an increase in the exposure time and the appearance of Zr-enriched regions is most clearly observed after 1000 h exposure. Nevertheless, some amount of yttrium and zirconium can be found in uncrystallized vitreous regions (Figure 10, Table S2) even in boron-free glasses, which allows one to expect Zr-containing phase formation with an increase in the exposure time.

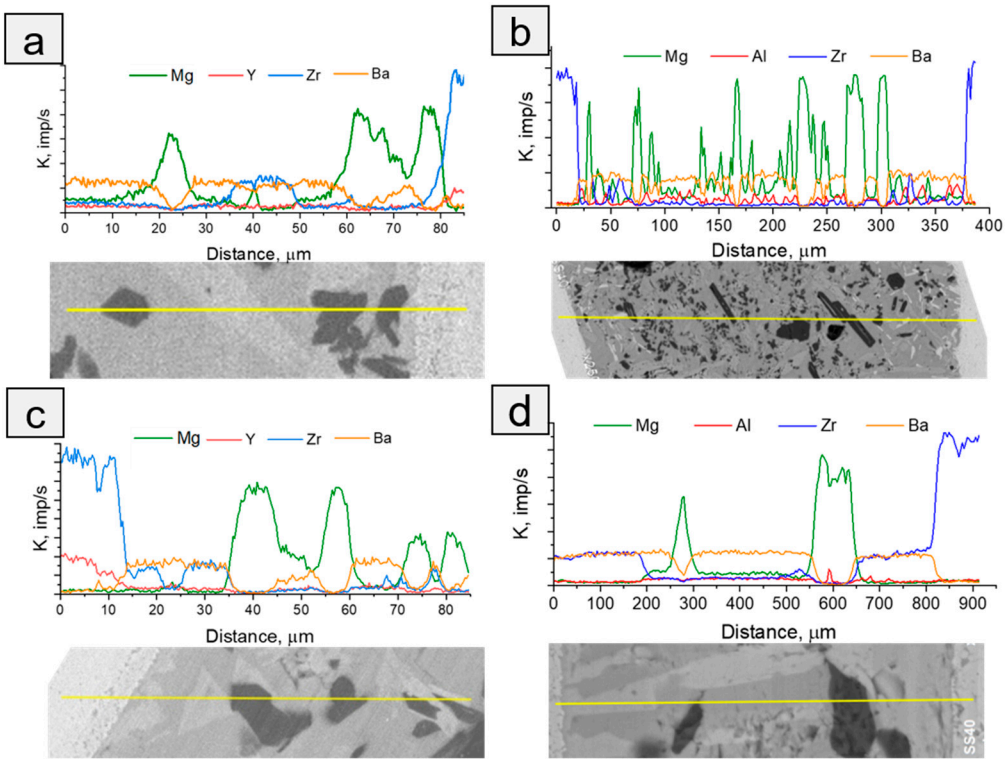

Figure 11. Element distribution over the YSZ–3B samples exposed for 125 (**a**), 500 (**c**), and 1000 h (**d**) at 1000 °C and YSZ–3A sample exposed for 1000 h (**b**).

Although Zr^{4+} and Y^{3+} diffusion into the sealant volume is well known for glasses containing barium and boron oxides [25,26,42,60], its mechanism has not been unambiguously explained yet. Moreover, less complex reaction products such as barium zirconate ($BaZrO_3$) [61] are typically formed. According to the $BaO–ZrO_2–SiO_2$ phase diagram [62], the $BaZrSi_3O_9$ compound can be obtained by the co-sintering of corresponding oxides at 1300 °C for 30 h, and it melts congruently at 1450 °C with the formation of $BaSi_2O_5$ and $ZrSiO_4$. However, there is some evidence that the $BaZrSi_3O_9$ phase can crystallize in glasses at temperatures below 1300 °C and much lower exposure times [63,64]. Preparing glass–ceramics using the unconventional solid-state method, Bo Li and co-authors suggest the following equation to describe the barium zirconium silicate formation: $BaO + ZrO_2 + 3SiO_2 = BaZrS_{i3}O_9$ [63,64], which is close to the one proposed by V. G. Chukhlantsev and Y. M. Galkin [62]. However, even though this equation appears to be suitable for ceramics and glass–ceramics obtained by sintering, it seems that it cannot be applied to describe the phase formation during glass crystallization due to the existence of an extended glass network.

In glasses similar to the ones studied in this work, BaO and SiO_2 can act as glass formers, MgO is a network modifier [65], and zirconium can be considered either as a glass former [66] or a modifier [67]. Therefore, it might be assumed that Zr^{4+} ions can embed into the Si-enriched part of the glass network forming $ZrSiO_4$ and then react with

the Ba-enriched part of the glass network, which could lead to the $BaZrS_{i3}O_9$ formation. V. G. Chukhlantsev and Y. M. Galkin [62] proved the possibility of $BaZrSi_3O_9$ formation through the sintering of $BaSi_2O_5$ + ZrO_2 and $BaSi_2O_5$ + $ZrSiO_4$ mixtures at 1250 °C for 80 h. Since the sintering of the $BaSi_2O_5$ + ZrO_2 mixture results in the formation of $Ba_2Zr_2Si_3O_{12}$ composition, which was not observed in the studied glass, it could be assumed that the barium zirconium silicate formation in the glass network might be described by the $BaSi_2O_5$ + $ZrSiO_4$ = $BaZrSi_3O_9$ equation.

Zr^{4+} and Y^{3+} diffusion did not worsen the integrity of YSZ–sealant joints and it did not affect the adhesion to ceramics, which allows the sealants to be applied for the sealing of zirconia-based ceramics. However, yttrium diffusion from YSZ to glass could cause cubic → monoclinic transition in ZrO_2 [68] and the degradation of its surface, which might lead to joint failure.

All glass sealants passed the long exposure tests and showed good results in adhesion and thermal compatibility with the electrolyte. The most suitable option for further application is aluminum-containing glass because only a slight Zr^{4+} diffusion was observed and they can be expected to provide good sealing at a longer operating time. It should be mentioned that the behavior of the studied glasses differs from some glasses studied before. For example, the formation of $BaMg_2Si_2O_7$ in the phase observed in this work is hardly discussed in the literature because the formation of $Ba_2Si_3O_8$, $BaSi_2O_5$, and $BaAl_2Si_2O_8$ phases is more typical for barium-containing glasses [42,43,53].

4. Conclusions

Glasses with different Al_2O_3 and B_2O_3 content were obtained in the $(50 - x)SiO_2$-30BaO-20MgO-xAl_2O_3/B_2O_3 (wt.%) system. An increase in B_2O_3 content results in a decrease in the glass transition temperature, while the introduction of Al_2O_3 has the opposite effect. The CTE values of the samples do not depend on the composition, which may be due to crystallization upon heating. This ensures the long-term stability of the sealant–YSZ joints.

The crystallization processes in the studied glasses strongly depend on the heat treatment temperature. Heat treatment at 1050 °C results in the formation of $BaMg_2Si_2O_7$, $MgSiO_3$, and Mg_2SiO_4 phases in all of the studied glass sealants. Al_2O_3-containing glasses show a higher tendency to crystallize.

According to SEM and EDX studies of the behavior of the glass sealant in contact with YSZ ceramics, a higher tendency of Zr^{4+} to diffuse from the ceramic into the glass volume is observed for B_2O_3-containing glasses after exposure at 1000 °C. This diffusion results in the formation of the $BaZrSi_3O_9$ phase throughout the sealant. The Zr^{4+} diffusion depth in Al_2O_3-containing glasses is much smaller.

It can be concluded that the 4A composition is the most suitable for application in high-temperature devices based on YSZ ceramics, including solid oxide fuel cells, electrolyzers, and gas sensors. Despite a greater crystallization tendency, the presence of Al_2O_3 significantly inhibits the diffusion of Zr^{4+}, ensuring the stability of the sealant–YSZ joints. This sealant composition was successfully used to create an oxygen pump with a sensor that operates for a long time at temperatures of 850–1100 °C (Figure S1).

Supplementary Materials: The following supporting information can be downloaded at: https://www.mdpi.com/article/10.3390/ceramics6030081/s1: Table S1. EDX results for spectra provided in Figures 7 and 8. Table S2. EDX results for spectra provided in Figure 11. Figure S1. Oxygen pump with sensor glued with glass sealant

Author Contributions: Conceptualization, A.V. and N.S.; methodology, A.V., D.D. and D.K.; formal analysis, N.S. and S.B.; investigation, S.B., A.V., Y.C. and D.K.; data curation, N.S.; writing—original draft preparation, A.V., N.S. and D.K.; writing—review and editing, A.V. and N.S.; visualization, A.V.; supervision, A.K.; project administration, A.K. All authors have read and agreed to the published version of the manuscript.

Funding: The study of the interaction between glass and ceramics was funded by the Russian Science Foundation, grant number 21-79-30051.

Institutional Review Board Statement: Not applicable.

Informed Consent Statement: Not applicable.

Data Availability Statement: The data presented in this study are available on request from the corresponding author.

Acknowledgments: The research was partially performed using the facilities of the Shared Access Centre "Composition of Compounds" of IHTE UB RAS. The authors are grateful to A. V. Khodimchuk for her kind assistance with the XRD experiments.

Conflicts of Interest: The authors declare no conflict of interest.

References

1. Cirera, A.; Lpez-Gándara, C.; Ramos, F.M. YSZ-based oxygen sensors and the use of nanomaterials: A review from classical models to current trends. *J. Sens.* **2009**, *2009*, 15. [CrossRef]
2. Muroyama, H.; Okuda, S.; Matsui, T.; Hashigami, S.; Kawano, M.; Inagaki, T.; Eguchi, K. Gas composition analysis using yttria-stabilized zirconia oxygen sensor during dry reforming and partial oxidation of methane. *J. Jpn. Pet. Inst.* **2018**, *61*, 72–79. [CrossRef]
3. Liu, M.; Dong, D.; Peng, R.; Gao, J.; Diwu, J.; Liu, X.; Meng, G. YSZ-based SOFC with modified electrode/electrolyte interfaces for operating at temperature lower than 650 °C. *J. Power Sources* **2008**, *180*, 215–220. [CrossRef]
4. Hauch, A.; Brodersen, K.; Chen, M.; Mogensen, M.B. Ni/YSZ electrodes structures optimized for increased electrolysis performance and durability. *Solid State Ion.* **2016**, *293*, 27–36. [CrossRef]
5. Jiang, L.; Lv, S.; Tang, W.; Zhao, L.; Wang, C.; Wang, J.; Wang, T.; Guo, X.; Liu, F.; Wang, C.; et al. YSZ-based acetone sensor using a Cd2SnO4 sensing electrode for exhaled breath detection in medical diagnosis. *Sens. Actuators B Chem.* **2021**, *345*, 130321. [CrossRef]
6. Miura, N.; Sato, T.; Anggraini, S.A.; Ikeda, H.; Zhuiykov, S. A review of mixed-potential type zirconia-based gas sensors. *Ionics* **2014**, *20*, 901–925. [CrossRef]
7. Tho, N.D.; Van Huong, D.; Ngan, P.Q.; Thai, G.H.; Thu, D.T.A.; Thu, D.T.; Tuoi, N.T.M.; Toan, N.N.; Giang, H.T. Effect of sintering temperature of mixed potential sensor Pt/YSZ/$LaFeO_3$ on gas sensing performance. *Sens. Actuators B Chem.* **2016**, *224*, 747–754. [CrossRef]
8. Wang, J.; Wang, C.; Liu, A.; You, R.; Liu, F.; Li, S.; Zhao, L.; Jin, R.; He, J.; Yang, Z.; et al. High-response mixed-potential type planar YSZ-based NO_2 sensor coupled with $CoTiO_3$ sensing electrode. *Sens. Actuators B Chem.* **2019**, *287*, 185–190. [CrossRef]
9. Schubert, F.; Wollenhaupt, S.; Kita, J.; Hagen, G.; Moos, R. Platform to develop exhaust gas sensors manufactured by glass-solder-supported joining of sintered yttria-stabilized zirconia. *J. Sens. Sens. Syst.* **2016**, *5*, 25–32. [CrossRef]
10. Zhang, X.D.; Li, J.J.; Guo, X. Oxygen pump based on stabilized zirconia. *Rev. Sci. Instrum.* **2015**, *86*, 115103. [CrossRef]
11. Tao, M.; Feng, J.; Li, R.; Guan, C.; Wang, J.; Chi, B.; Pu, J. Interfacial compatibility and thermal cycle stability for glass-sealed oxygen sensors. *Ceram. Int.* **2023**, *49*, 23180–23188. [CrossRef]
12. Spirin, A.; Lipilin, A.; Ivanov, V.; Paranin, S.; Nikonov, A.; Khrustov, V.; Portnov, D.; Gavrilov, N.; Mamaev, A. Solid Oxide Electrolyte Based Oxygen Pump. In Proceedings of the 12th International Ceramics Congress Part D, Montecatini Terme, Italy, 6–11 June 2010; Volume 65, pp. 257–262.
13. Spirin, A.V.; Nikonov, A.V.; Lipilin, A.S.; Paranin, S.N.; Ivanov, V.V.; Khrustov, V.R.; Valentsev, A.V.; Krutikov, V.I. Electrochemical cell with solid oxide electrolyte and oxygen pump thereof. *Russ. J. Electrochem.* **2011**, *47*, 569–578. [CrossRef]
14. Pham, A.Q.; Glass, R.S. Oxygen pumping characteristics of yttria-stabilized-zirconia. *Electrochim. Acta.* **1998**, *43*, 2699–2708. [CrossRef]
15. Khodimchuk, A.V.; Anan'ev, M.V.; Eremin, V.A.; Tropin, E.S.; Farlenkov, A.S.; Porotnikova, N.M.; Kurumchin, E.K.; Bronin, D.I. Oxygen isotope exchange between the gas-phase and the electrochemical cell O_2, Pt | YSZ | Pt, O_2 under conditions of applied potential difference. *Russ. J. Electrochem.* **2017**, *53*, 838–845. [CrossRef]
16. Gunduz, S.; Dogu, D.; Deka, D.J.; Meyer, K.E.; Fuller, A.; Co, A.C.; Ozkan, U.S. Application of solid electrolyte cells in ion pump and electrolyzer modes to promote catalytic reactions: An overview. *Catal. Today* **2019**, *323*, 3–13. [CrossRef]
17. Sohn, S.B.; Choi, S.Y.; Kim, G.H.; Song, H.S.; Kim, G.D. Suitable Glass-Ceramic Sealant for Planar Solid-Oxide Fuel Cells. *J. Am. Ceram. Soc.* **2004**, *87*, 254–260. [CrossRef]
18. Batfalsky, P.; Haanappel, V.A.C.; Malzbender, J.; Menzler, N.H.; Shemet, V.; Vinke, I.C.; Steinbrech, R.W. Chemical interaction between glass-ceramic sealants and interconnect steels in SOFC stacks. *J. Power Sources* **2006**, *155*, 128–137. [CrossRef]
19. Wang, X.; Yan, D.; Fang, D.; Luo, J.; Pu, J.; Chi, B.; Jian, L. Optimization of Al2O3-glass composite seals for planar intermediate-temperature solid oxide fuel cells. *J. Power Sources* **2013**, *226*, 127–133. [CrossRef]
20. Singh, K.; Walia, T. Review on silicate and borosilicate-based glass sealants and their interaction with components of solid oxide fuel cell. *Int. J. Energy Res.* **2021**, *45*, 20559–20582. [CrossRef]

21. Meinhardt, K.D.; Kim, D.S.; Chou, Y.S.; Weil, K.S. Synthesis and properties of a barium aluminosilicate solid oxide fuel cell glass-ceramic sealant. *J. Power Sources* **2008**, *182*, 188–196. [CrossRef]
22. Mahapatra, M.K.; Lu, K. Glass-based seals for solid oxide fuel and electrolyzer cells—A review. *Mater. Sci. Eng. R Reports* **2010**, *67*, 65–85. [CrossRef]
23. Kosiorek, M.; Żurawska, A.; Ajdys, L.; Kolasa, A.; Naumovich, Y.; Wiecińska, P.; Yaremchenko, A.; Kupecki, J. Glass–Zirconia Composites as Seals for Solid Oxide Cells: Preparation, Properties, and Stability over Repeated Thermal Cycles. *Materials* **2023**, *16*, 1634. [CrossRef] [PubMed]
24. Wang, X.; Li, R.; Yang, J.; Gu, D.; Yan, D.; Pu, J.; Chi, B.; Li, J. Effect of YSZ addition on the performance of glass-ceramic seals for intermediate temperature solid oxide fuel cell application. *Int. J. Hydrog. Energy* **2018**, *43*, 8040–8047. [CrossRef]
25. Kumar, V.; Kaur, G.; Pandey, O.P.; Singh, K.; Lu, K. Effect of Thermal Treatment on Chemical Interaction Between Yttrium Borosilicate Glass Sealants and YSZ for Planar Solid Oxide Fuel Cells. *Int. J. Appl. Glas. Sci.* **2014**, *5*, 410–420. [CrossRef]
26. Kaur, G.; Pandey, O.P.; Singh, K. Chemical compatibility between MgO-SiO_2-B_2O_3-La_2O_3 glass sealant and low, high temperature electrolytes for solid oxide fuel cell applications. *Int. J. Hydrog. Energy* **2012**, *37*, 17235–17244. [CrossRef]
27. Smeacetto, F.; Salvo, M.; Ferraris, M.; Cho, J.; Boccaccini, A.R. Glass-ceramic seal to join Crofer 22 APU alloy to YSZ ceramic in planar SOFCs. *J. Eur. Ceram. Soc.* **2008**, *28*, 61–68. [CrossRef]
28. Sabato, A.G.; Rost, A.; Schilm, J.; Kusnezoff, M.; Salvo, M.; Chrysanthou, A.; Smeacetto, F. Effect of electric load and dual atmosphere on the properties of an alkali containing diopside-based glass sealant for solid oxide cells. *J. Power Sources* **2019**, *415*, 15–24. [CrossRef]
29. Ferraris, M.; De la Pierre, S.; Sabato, A.G.; Smeacetto, F.; Javed, H.; Walter, C.; Malzbender, J. Torsional shear strength behavior of advanced glass-ceramic sealants for SOFC/SOEC applications. *J. Eur. Ceram. Soc.* **2020**, *40*, 4067–4075. [CrossRef]
30. Li, R.; Liang, X.; Wang, X.; Zeng, W.; Yang, J.; Yan, D.; Pu, J.; Chi, B.; Li, J. Improvement of sealing performance for Al2O3 fiber-reinforced compressive seals for intermediate temperature solid oxide fuel cell. *Ceram. Int.* **2019**, *45*, 21953–21959. [CrossRef]
31. Zhang, W.; Wang, X.; Dong, Y.; Yang, J.J.; Pu, J.; Chi, B.; Jian, L. Development of flexible ceramic-glass seals for intermediate temperature planar solid oxide fuel cell. *Int. J. Hydrog. Energy* **2016**, *41*, 6036–6044. [CrossRef]
32. Krainova, D.A.; Saetova, N.S.; Kuzmin, A.V.; Raskovalov, A.A.; Eremin, V.A.; Ananyev, M.V.; Steinberger-Wilckens, R. Non-crystallising glass sealants for SOFC: Effect of Y_2O_3 addition. *Ceram. Int.* **2020**, *46*, 5193–5200. [CrossRef]
33. Krainova, D.A.; Saetova, N.S.; Polyakova, I.G.; Farlenkov, A.S.; Zamyatin, D.A.; Kuzmin, A.V. Behaviour of $54.4SiO_2$-$13.7Na_2O$-$1.7K_2O$-$5.0CaO$-$12.4MgO$-$0.6Y_2O_3$-$11.3Al_2O_3$-$0.9B_2O_3$ HT-SOFC glass sealant under oxidising and reducing atmospheres. *Ceram. Int.* **2022**, *48*, 6124–6130. [CrossRef]
34. Krainova, D.A.; Saetova, N.S.; Farlenkov, A.S.; Khodimchuk, A.V.; Polyakova, I.G.; Kuzmin, A.V. Long-term stability of SOFC glass sealant under oxidising and reducing atmospheres. *Ceram. Int.* **2021**, *47*, 8973–8979. [CrossRef]
35. Saetova, N.S.; Krainova, D.A.; Kuzmin, A.V.; Raskovalov, A.A.; Zharkinova, S.T.; Porotnikova, N.M.; Farlenkov, A.S.; Moskalenko, N.I.; Ananyev, M.V.; Dyadenko, M.V.; et al. Alumina–silica glass–ceramic sealants for tubular solid oxide fuel cells. *J. Mater. Sci.* **2019**, *54*, 4532–4545. [CrossRef]
36. Kaur, G. *Solid Oxide Fuel Cell Components: Seal Glass for Solid Oxide Fuel Cells*; Springer: Berlin/Heidelberg, Germany, 2016; Volume 58, ISBN 978-3-319-25596-5.
37. Walia, T.; Singh, K. Mixed alkaline earth modifiers effect on thermal, optical and structural properties of SrO-BaO-SiO_2-B_2O_3-ZrO_2 glass sealants. *J. Non. Cryst. Solids* **2021**, *564*, 120812. [CrossRef]
38. Kaur, G.; Pandey, O.P.; Singh, K. Effect of modifiers field strength on optical, structural and mechanical properties of lanthanum borosilicate glasses. *J. Non. Cryst. Solids* **2012**, *358*, 2589–2596. [CrossRef]
39. Rodríguez-López, S.; Wei, J.; Laurenti, K.C.; Mathias, I.; Justo, V.M.; Serbena, F.C.; Baudín, C.; Malzbender, J.; Pascual, M.J. Mechanical properties of solid oxide fuel cell glass-ceramic sealants in the system BaO/SrO-MgO-B_2O_3-SiO_2. *J. Eur. Ceram. Soc.* **2017**, *37*, 3579–3594. [CrossRef]
40. Lim, E.S.; Kim, B.S.; Lee, J.H.; Kim, J.J. Effect of BaO content on the sintering and physical properties of BaO-B_2O_3-SiO_2 glasses. *J. Non. Cryst. Solids* **2006**, *352*, 821–826. [CrossRef]
41. QI, S.; Portnikova, N.M.; Ananyev, M.V.; Kuzmin, A.V.; Eremin, V.A. High-temperature glassy-ceramic sealants SiO_2—Al_2O_3—BaO—MgO and SiO_2—Al_2O_3—ZrO_2—CaO—Na_2O for solid oxide electrochemical devices. *Trans. Nonferrous Met. Soc. China* **2016**, *26*, 2916–2924. [CrossRef]
42. Kaur, N.; Kaur, G.; Kumar, D.; Singh, K. Mechanical and thermal properties of SrO/BaO modified Y_2O_3-Al_2O_3-B_2O_3-SiO_2 glasses and their compatibility with solid oxide fuel cell components. *J. Phys. Chem. Solids* **2018**, *118*, 248–254. [CrossRef]
43. Rezazadeh, L.; Hamnabard, Z.; Baghshahi, S.; Golikand, A.N. Adhesion and interfacial interactions of BaO–SiO_2–B_2O_3-based glass-ceramic seals and AISI430 interconnect for solid oxide fuel cell applications. *Ionics* **2016**, *22*, 1899–1908. [CrossRef]
44. Navarro-Pardo, F.; Martínez-Barrera, G.; Martínez-Hernández, A.L.; Castaño, V.M.; Rivera-Armenta, J.L.; Medellín-Rodríguez, F.; Velasco-Santos, C. Effects on the thermo-mechanical and crystallinity properties of nylon 6,6 electrospun fibres reinforced with one dimensional (1D) and two dimensional (2D) carbon. *Materials* **2013**, *6*, 3494–3513. [CrossRef] [PubMed]
45. Kerstan, M.; Müller, M.; Rüssel, C. Thermal expansion of $Ba_2ZnSi_2O_7$, $BaZnSiO_4$ and the solid solution series $BaZn_2$-$xMgxSi_2O_7$ ($0 \leq x \leq 2$) studied by high-temperature X-ray diffraction and dilatometry. *J. Solid State Chem.* **2012**, *188*, 84–91. [CrossRef]
46. Saetova, N.S.; Krainova, D.A.; Kuzmin, A.V. Effect of rare-earth oxides on thermal behavior of alumina-silica glass sealants. *J. Phys. Conf. Ser.* **2021**, *1967*, 012006. [CrossRef]

47. Smiljanić, S.V.; Grujić, S.R.; Tošić, M.B.; Živanović, V.D.; Stojanović, J.N.; Matijašević, S.D.; Nikolić, J.D. Crystallization and sinterability of glass-ceramics in the system La_2O_3-SrO-B_2O_3. *Ceram. Int.* **2014**, *40*, 297–305. [CrossRef]
48. Puig, J.; Ansart, F.; Lenormand, P.; Conradt, R.; Gross-Barsnick, S.M. Development of barium boron aluminosilicate glass sealants using a sol–gel route for solid oxide fuel cell applications. *J. Mater. Sci.* **2016**, *51*, 979–988. [CrossRef]
49. Goel, A.; Reddy, A.A.; Pascual, M.J.; Gremillard, L.; Malchere, A.; Ferreira, J.M.F. Sintering behavior of lanthanide-containing glass-ceramic sealants for solid oxide fuel cells. *J. Mater. Chem.* **2012**, *22*, 10042–10054. [CrossRef]
50. Saetova, N.S.; Shirokova, E.S.; Krainova, D.A.; Chebykin, N.S.; Ananchenko, B.A.; Tolstobrov, I.V.; Belozerov, K.S.; Kuzmin, A.V. The development of 3D technology for the creation of glass sealants for tubular oxide fuel cells. *Int. J. Appl. Glas. Sci.* **2022**, *13*, 684–694. [CrossRef]
51. Ghosh, S.; Kundu, P.; Das Sharma, A.; Basu, R.N.; Maiti, H.S. Microstructure and property evaluation of barium aluminosilicate glass-ceramic sealant for anode-supported solid oxide fuel cell. *J. Eur. Ceram. Soc.* **2008**, *28*, 69–76. [CrossRef]
52. Peng, L.; Zhu, Q.S. Thermal cycle stability of BaO-B_2O_3-SiO_2 sealing glass. *J. Power Sources* **2009**, *194*, 880–885. [CrossRef]
53. Da Silva, M.J.; Bartolomé, J.F.; De Aza, A.H.; Mello-Castanho, S. Glass ceramic sealants belonging to BAS (BaO-Al_2O_3-SiO_2) ternary system modified with B2O3 addition: A different approach to access the SOFC seal issue. *J. Eur. Ceram. Soc.* **2016**, *36*, 631–644. [CrossRef]
54. Li, X.; Yazhenskikh, E.; Groß-Barsnick, S.M.; Baumann, S.; Behr, P.; Deibert, W.; Koppitz, T.; Müller, M.; Meulenberg, W.A.; Natour, G. Crystallization behavior of BaO–CaO–SiO_2–B_2O_3 glass sealant and adjusting its thermal properties for oxygen transport membrane joining application. *J. Eur. Ceram. Soc.* **2023**, *43*, 2541–2552. [CrossRef]
55. Craievich, A.F.; Zanotto, E.E.; James, P.F. Kinetics of sub-liquidus phase separation in silicate and borate glasses. A review. *Bull. Mineral.* **1983**, *106*, 169–184. [CrossRef]
56. Abdel-Hameed, S.A.M.; Abo-Naf, S.M.; Hamdy, Y.M. The effect of heat treatment on photoluminescence and magnetic properties of new yellow phosphor based on sanbornite ($BaSi_2O_5$) glass ceramic doped with Gd^{3+} and Mn^{2+}. *J. Non. Cryst. Solids* **2019**, *517*, 106–113. [CrossRef]
57. Saxena, S.K.; Chatterjee, N.; Fei, Y.; Shen, G. *Thermodynamic Data on Oxides and Silicates: An Assessed Data Set Based on Thermochemistry and High Pressure Phase Equilibrium*; Springer: Berlin/Heidelberg, Germany, 1993; ISBN 3642783325.
58. Decterov, S.A.; Jung, I.-H.; Pelton, A.D. Thermodynamic Modeling of the FeO-Fe_2O_3-MgO-SiO_2 System. *J. Am. Ceram. Soc.* **2002**, *85*, 2903–2910. [CrossRef]
59. Jung, I.H.; Decterov, S.A.; Pelton, A.D.; Kim, H.M.; Kang, Y.B. Thermodynamic evaluation and modeling of the Fe-Co-O system. *Acta. Mater.* **2004**, *52*, 507–519. [CrossRef]
60. Kaur, G.; Singh, K.; Pandey, O.P. Investigations on Interfacial Interaction of Glass Sealants with Electrolytes and Interconnect for Solid Oxide Fuel Cells. Ph.D. Thesis, Thapar University, Punjab, India, 2012.
61. Brochu, M.; Gauntt, B.D.; Shah, R.; Miyake, G.; Loehman, R.E. Comparison between barium and strontium-glass composites for sealing SOFCs. *J. Eur. Ceram. Soc.* **2006**, *26*, 3307–3313. [CrossRef]
62. Chukhlantsev, V.G.; Yu, M. Galkin Study of the BaO-ZrO_2-SiO_2 System at Subsolidus temperatures. *Dokl. Akad. Nauk. SSSR* **1968**, *168–169*, 128.
63. Li, B.; Tang, B.; Xu, M. Influences of CaO on Crystallization, Microstructures, and Properties of BaO-Al_2O_3-B_2O_3-SiO_2 Glass–Ceramics. *J. Electron. Mater.* **2015**, *44*, 3849–3854. [CrossRef]
64. Li, B.; Xu, M.; Tang, B. Effects of ZnO on crystallization, microstructures and properties of BaO–Al_2O_3–B_2O_3–SiO_2 glass–ceramics. *J. Mater. Sci. Mater. Electron.* **2016**, *27*, 70–76. [CrossRef]
65. Kermani, P.S.; Ghatee, M.; Sirr Irvine, J.T. Characterization of a barium-calcium-aluminosilicate glass/fiber glass composite seal for intermediate temperature solid oxide fuel cells. *Bol. La Soc. Esp. Ceram. Y Vidr.* **2022**, in press. [CrossRef]
66. Lu, X.; Deng, L.; Kerisit, S.; Du, J. Structural role of ZrO_2 and its impact on properties of boroaluminosilicate nuclear waste glasses. *Npj Mater. Degrad.* **2018**, *2*, 19. [CrossRef]
67. Khan, S.; Kaur, G.; Singh, K. Effect of ZrO_2 on dielectric, optical and structural properties of yttrium calcium borosilicate glasses. *Ceram. Int.* **2017**, *43*, 722–727. [CrossRef]
68. Chen, S.; Yu, Z.; Zhang, Q.; Wang, J.; Zhang, T.; Wang, J. Reducing the interfacial reaction between borosilicate sealant and yttria-stabilized zirconia electrolyte by addition of HfO_2. *J. Eur. Ceram. Soc.* **2015**, *35*, 2–6. [CrossRef]